International Journal of Automotive Technology, Vol. 6, No. 6, pp. 643–655 (2005)

1229-9138/2005/024-12

EFFECTIVE REINFORCEMENT OF S-SHAPED FRONT FRAME WITH A CLOSED-HAT SECTION MEMBER FOR FRONTAL IMPACT USING HOMOGENIZATION METHOD

Y.-B. CHO[1)], M.-W. SUH[2)*] and H.-C. SIN[3)]

[1)]TNO Automotive Korea Ltd., Rm 1810, LG Twintel 2, 157-3 Samsung-dong, Gangnam-gu, Seoul 135-880, Korea
[2)]School of Mechanical Engineering, Sungkyunkwan University, Suwon, Gyeonggi 440-746, Korea
[3)]School of Mechanical and Aerospace Engineering, Seoul National University, Seoul 151-742, Korea

(Received 22 October 2004; Revised 4 February 2005)

ABSTRACT–The frontal crash optimization of S-shaped closed-hat section member using the homogenization method, design of experiment (DOE) and response surface method (RSM) was studied. The optimization to effectively absorb more crash energy was studied to introduce the reinforcement design. The main focus of design was to decide the optimum size and thickness of reinforcement. In this study, the location of reinforcement was decided by homogenization method. Also, the effective size and thickness of reinforcements was studied by design of experiments and response surface method. The effects of various impact velocity for reinforcement design were researched. The high impact velocity reinforcement design showed to absorb the more crash energy than low velocities design. The effect of size and thickness of reinforcement was studied and the sensitivity of size and thickness was different according to base thickness of model. The optimum size and thickness of the reinforcement has shown a direct proportion to the thickness of base model. Also, the thicker the base model was, the effect of optimization using reinforcement was the bigger. The trend curve for effective size and thickness of reinforcement using response surface method was obtained. The predicted size and thickness of reinforcement by RSM were compared with results of DOE. The results of a specific dynamic mean crushing loads for the predicted design by RSM were shown the small difference with the predicted results by RSM and DOE. These trend curves can be used as a basic guideline to find the optimum reinforcement design for S-shaped member.

KEY WORDS : Optimum reinforcement design, S-shaped member, Homogenization method, design of experiment (DOE), response surface method (RSM)

1. INTRODUCTION

The front frame of a vehicle with a closed-hat section, which constitutes the main structural members to absorb the vehicle crash energy, usually has an S-shape because of the interference with the other components such as engine, transmission, drive train, suspension assembly and etc. This S-shape generates an unexpected bending deformation instead of axial crushing, causing the absorbing capacity of crash energy to decrease.

Therefore, in order to upgrade a capacity of absorbing crash energy, an easy and efficient method to reinforce poor bending deformation should be studied.

To this end, many researches on the absorption of more crash energy have been conducted. Wang and Meredith (1994) carried out experimental and numerical studies of the bending-buckling behaviors with rectangular section S-shaped torque box beam. The cases of un-reinforced, partially reinforced and fully reinforced were also investigated.

Ohkami *et al.* (1990) and Abe *et al.* (1990) studied the collapse characteristics of thin-walled curved beams with closed-hat section under axial compression load using static dynamic collapsing tests. Also, the calculated results, which was predicted by the elastic-plastic structural analysis method, and experimental results of deformed shapes of beams, the local buckling modes and the force-displacement relations were compared.

Drazetic *et al.* (1993) conducted studies on the rapid estimate using kinematical models of an S-shape frame undergoing a collision against a rigid wall and compared the experimental test results and the numerical calculations.

H. S. Kim *et al.* (2001) studied the effect of cross-sectional shape of hat-type cross-section on crash resistance of an S-frame model with diagonally positioned internal stiffener and triggering dents using numerical simulation. It was reported that in some cases, energy of

*Corresponding author. e-mail: suhmw@yurim.skku.ac.kr

more than 200% could be absorbed than the conventional double-hat/double-cell profile member.

Elmalakbi and Zu (2004) proposed vehicle smart structures that front-end structure consists of two hydraulic cylinders integrated with the front-end longitudinal members of standard vehicles. The work carried out in this paper included developing and analyzing mathematical models of two different cases representing vehicle-to-vehicle and vehicle-to-barrier in full and offset collisions. The smart structures showed significantly lower intrusions and decelerations.

Mayor (1994, 1996) applied the homogenization method (Bendsoe and Kikuchi, 1988; Guedes and Kikuchi, 1990; Suzuki and Kikuchi, 1991; Min and Kikuchi, 1997) to increase crash energy absorption for a rear impact subsystem model by inducing an artificial axial collapse that were induced by hole of which the elements were lower than given threshold value. Ma *et al.* (2004) demonstrated a structural crashworthiness design process employing a multi-domain and multi-step topology optimization approach using 2-D and 3-D real vehicle structure. The proposed new design is checker board pattern is not easy for automotive manufacturing process. Qi *et al.* (2005) studied a step by step failure modification approach using static topology analysis for crashworthiness design problem.

In this paper, in order to reinforce poor bending deformation of S-shaped closed-hat section member in frontal crash, the numerical method using the homogenization method, the DOE method (Taguchi, 1987; Phadke, 1989) and the RSM method (Myers, 1971) was studied. The method for absorbing more crash energy was studied to introduce the reinforcement on easily deforming area. The location of the reinforcement was decided by the homogenization method. The highly strained elements of the front frame were become the reinforcement instead of the Mayor's proposal that low strained elements become the deleted elements (Cho, 2001; 2002).

In this research, the effect of the size and thickness of reinforcements to the level of absorption of crash energy were studied. Second, the effects of various impact velocities for the reinforcement design were studied. Third, the optimum size and thickness of reinforcements according to various thicknesses were studied using the DOE and RSM methods. The trend curve to easily predict the effective size and thickness of the reinforcement was studied using response surface method and the predicted dynamic mean crushing loads were compared to the confirmed analysis results.

2. THE HOMOGENIZATION METHOD

The objective of the research is to maximize the internal energy at the final time step, t_f. This can be expressed as

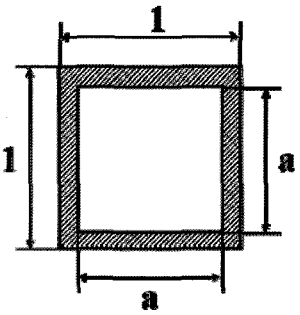

Figure 1. Plane stress unit cell.

$$U = \int_{\Omega} \frac{1}{2} E_{ijkl} \frac{\partial u_i}{\partial x_j} \frac{\partial u_k}{\partial x_l} dx|_{t=t_f} \tag{1}$$

The homogenization method (Mayor, 1994; 1996) is applied to the objective function, which can be expressed as

$$U^H(\mu) = \int_{\Omega} \frac{1}{2} E^H_{ijkl} \frac{\partial u_i}{\partial x_j} \frac{\partial u_k}{\partial x_l} dx|_{t=t_f} \tag{2}$$

The in-plane stress density, μ, of a square unit cell is defined by

$$\mu = 1 - a^2 \tag{3}$$

In previous work, the homogenized modules, E^H_{ijkl}, were approximated as a function of density, $E_{ijkl}\mu^6$ (Mayor, 1994).

A realistic problem requires some constraint on the material. The volume, $V(\mu)$, is a function of the microstructure design variables and is restricted to be less than some maximum value, $\bar{V}$.

$$\int_{\Omega} V(\mu) dx - \bar{V} \le 0 \tag{4}$$

The design variable density, μ, is constrained by

$$0 \le \mu \le 1 \tag{5}$$

At some time, t_1, the optimized design may have a total internal energy that is larger than the optimized total internal energy of the later time t_f. This may occur if a structure is both stiff and highly energy absorbent.

To take advantage of the potential improvement in energy absorption at earlier stages, the objective function is modified using weighting factors, which are W_1, W_2, ...W_n, for the energy at each time step.

$$\begin{aligned} \max_{\mu} \{ & W_1 [\int_{\Omega} \frac{1}{2} E^H_{ijkl}(\mu) \frac{\partial u_i}{\partial x_j} \frac{\partial u_k}{\partial x_l} dx|_{t=t_1}] \\ & + W_2 [\int_{\Omega} \frac{1}{2} E^H_{ijkl}(\mu) \frac{\partial u_i}{\partial x_j} \frac{\partial u_k}{\partial x_l} dx|_{t=t_2}] + \cdots \end{aligned} \tag{6}$$

If the structure is divided into finite elements (using

superscript (e) to designate the element values), then the optimality criteria (Mayor, 1994) can be shown to be

$$\Lambda_V^e = \frac{W_1 \int_{v^{(e)}} \frac{dU^H}{d\mu^{(e)}}|_{t=t_1} dV^{(e)} + W_2 \int_{v^{(e)}} \frac{dU^H}{d\mu^{(e)}}|_{t=t_2} dV^{(e)} + \cdots}{\int_{v^{(e)}} \frac{dV}{d\mu^{(e)}} dV^{(e)}} = const. \quad (7)$$

where

$$\frac{dU^H}{d\mu^{(e)}} = \frac{dE^H_{ijkl}}{d\mu^{(e)}} \frac{\partial u_i}{\partial x_j} \frac{\partial u_k}{\partial x_l}$$

The volume constraint is specified as a percentage of the original volume with no holes, and is termed volume fraction (VF).

$$VF \equiv \frac{\bar{V}}{V_o} = \frac{\bar{V}}{\int_V V_{\mu=1} dV} \quad (8)$$

To maximize the internal energy of the structure, the elements with a low $\Lambda^{(e)}$ value are eliminated. The new design with holes can lead to axial collapse. The resizing and threshold algorithms (Mayor, 1994; 1996) are used to decide the elements to be deleted.

Output files of used commercial program contains only maximum and minimum plastic strains of each element at the specified times. These strains are assumed constant throughout the area, $A^{(e)}$, of the element and vary only through the thickness, h, of the element. Therefore, the terms of equation (7) become the following equations.

$$\int_{V^{(e)}} \frac{dU^H}{d\mu} dV^{(e)} = A^{(e)} \int_{-h/2}^{h/2} dU^H dZ \quad (9)$$

$$\int_{V^{(e)}} \frac{\partial V(\mu)}{\partial \mu} dV^{(e)} = A^{(e)} \int_{-h/2}^{h/2} \frac{\partial V(\mu)}{\partial \mu} dZ \quad (10)$$

In microstructure, $\partial V(\mu)/\partial \mu$ becomes 1 by definition, where

$$\frac{\partial V(\mu)}{\partial \mu} = 1 \quad (11)$$

Using equation (9), (10) and (11), the optimality criteria of equation (7) is given by

$$\Lambda_V^{(e)} = W_1 \int_{-h/2}^{h/2} \frac{dU^H}{d\mu}\bigg|_{t=t_1} + W_2 \int_{-h/2}^{h/2} \frac{dU^H}{d\mu}\bigg|_{t=t_2} + \cdots = constant \quad (12)$$

where W_i is the weighting factor at specific time.

The term of the homogenized internal energy, U^H, is made of elastic internal energy, U^E and plastic energy, U^P. But, generally, in crash analysis, the elastic energy much less than the plastic energy, therefore U^H are approximated to U^P. The homogenized internal energy is given by

$$\begin{aligned} U^H &= U^E + U^P = \frac{1}{2} E^H_{ijkl} \varepsilon_{ij} \varepsilon_{kl} + \sigma^H_y \varepsilon_P + \frac{1}{2} E^H_P (\varepsilon_P)^2 \\ &\approx \sigma^H_y \varepsilon_P + \frac{1}{2} E^H_P (\varepsilon_P)^2 \end{aligned} \quad (13)$$

The derivation of equation (13) are given by

$$\frac{dU^H}{d\mu} = \frac{dU^H(\sigma^H_y \varepsilon_P)}{d\mu} + \frac{1}{2} \frac{dU^H[E^H_P(\varepsilon_P)^2]}{d\mu} \quad (14)$$

$$\frac{dU^H(\sigma^H_y \varepsilon_P)}{d\mu} = \left(\frac{1}{\sqrt{1-\mu}}\right) \sigma_y \varepsilon_P \quad (15)$$

$$\frac{dU^H[E^H_P(\varepsilon_P)^2]}{d\mu} = 6\mu^5 E_P (\varepsilon_P)^2 \quad (16)$$

If the plastic strains are bi-linear through thickness, then these are given by

$$\varepsilon_P = -z\left[\frac{\varepsilon^B_P - \varepsilon^M_P}{h/2}\right] + \varepsilon^M_P \qquad \text{-h/2} \le z \le 0 \quad (17)$$

$$\varepsilon_P = -z\left[\frac{\varepsilon^M_P - \varepsilon^T_P}{h/2}\right] + \varepsilon^M_P \qquad 0 \le z \le h/2 \quad (18)$$

where ε^B_P is plastic strain at bottom of plate, ε^M_P is plastic strain at middle of plate and ε^T_P is plastic strain at top of plate.

Using equations (15), (16), (17) and (18), equations (9) and (10) become

$$\begin{aligned} \int_{-h/2}^{h/2} \frac{dU^H[E^H(\varepsilon_P)^2]}{d\mu} dz = (6\mu^5) \frac{h^{(e)} E_P}{12} &[(\varepsilon^T_P)^2 + (\varepsilon^B_P)^2 \\ &+ 2(\varepsilon^M_P)^2 + (\varepsilon^M_P)(\varepsilon^B_P) + (\varepsilon^T_p)(\varepsilon^M_p)] \end{aligned} \quad (19)$$

$$\int_{-h/2}^{h/2} \frac{dU^H[\sigma^H_y \varepsilon_P]}{d\mu} dz = \left(\frac{1}{\sqrt{1-\mu}}\right) \frac{h^{(e)} \sigma^H_y}{4} [\varepsilon^T_P + 2(\varepsilon^M_P) + \varepsilon^B_P] \quad (20)$$

In the actual analysis, the crash program only yields the maximum plastic strain, $\varepsilon^{\max}_P$, and the minimum plastic strain, $\varepsilon^{\min}_P$. If these two strain are assumed ε^T_P and ε^B_P, then, ε^M_P is given by

$$\varepsilon^M_P = \frac{\varepsilon^{\max}_P + \varepsilon^{\min}_P}{2} \quad (21)$$

With these assumption, equations (19) and (20) can be expressed as

$$\begin{aligned} \int_{-h/2}^{h/2} \frac{dU^H[E^H(\varepsilon_P)^2]}{d\mu} dz = (6\mu^5) \frac{h^{(e)} E_P}{6} &[(\varepsilon^{\max}_P)^2 \\ &+ (\varepsilon^{\max}_P)(\varepsilon^{\min}_P) + (\varepsilon^{\min}_P)^2] \end{aligned} \quad (22)$$

$$\int_{-h/2}^{h/2} \frac{dU^H[\sigma^H_y \varepsilon_P]}{d\mu} dz = \left(\frac{1}{\sqrt{1-\mu}}\right) \frac{h^{(e)} \sigma^H_y}{2} [\varepsilon^{\max}_P + \varepsilon^{\min}_P] \quad (23)$$

The optimality criteria in equation (12) without the

weighting factor is given by

$$\Lambda_V^{(e)} = \frac{1}{2}\left[\mu^5 h^{(e)} E_P\{(\varepsilon_P^{\max})^2 + (\varepsilon_P^{\max})(\varepsilon_P^{\min}) + (\varepsilon_P^{\min})^2\} + \left(\frac{1}{\sqrt{1-\mu}}\right) h^{(e)} \sigma_y^H (\varepsilon_P^{\max} + \varepsilon_P^{\min})\right] \quad (24)$$

A resizing algorithm is used to satisfy the optimality criteria. The design variables, which are the element densities, $\mu^{(e)}$, and are changed to satisfy the optimality criteria. The strains are read from the crash analysis, and are unchanged during resizing.

$$\Lambda_{ave} = \frac{\sum_{e=1}^{n} \Lambda^{(e)}}{n} \quad (25)$$

First, in the resizing algorithm (Mayer, 1994) the average, Λ_{ave}, is obtained by summing the $\Lambda^{(e)}$ values for each element.

Because the range of $\Lambda^{(e)}$ for an elastic-plastic material is much larger than that of an elastic material, it was found that a resizing algorithm was needed where numerical constants were introduced to allow convergence (Mayer, 1994; 1996),

$$\mu_{k+1}^{(e)} = \left(\frac{\Lambda^{(e)}}{\Lambda_{ave}}\right)^{\beta_1} \mu_k^{(e)} \quad (26)$$

$$\text{If } \mu_{k+1}^{(e)} > \mu_k^{(e)} + \beta_2, \text{ then } \mu_{k+1}^{(e)} = \mu_k^{(e)} + \beta_2 \quad (27)$$

The first numerical constant, β_1, is less than 1, and this has the effect of limiting changes to the densities in a given step. The second condition requires the change in density for a given step to be at most β_2.

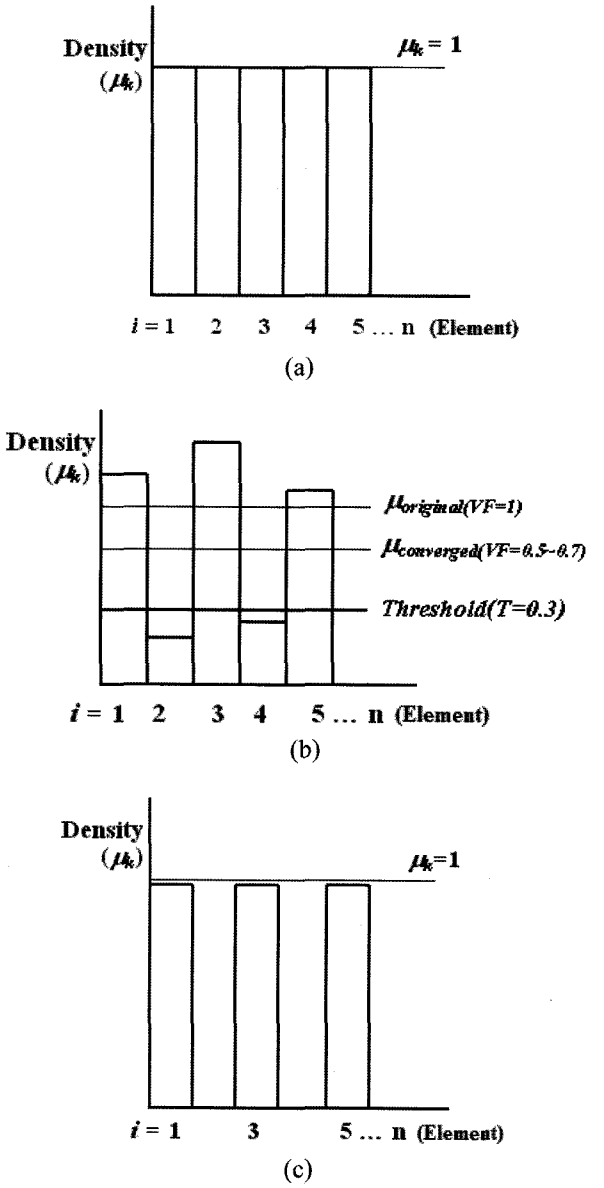

Figure 2. Resizing and threshold algorithm of Mayer's method: (a) Before resizing algorithm; (b) After resizing algorithm; (c) New designs that elements (2, 4) below threshold value were deleted after threshold algorithm.

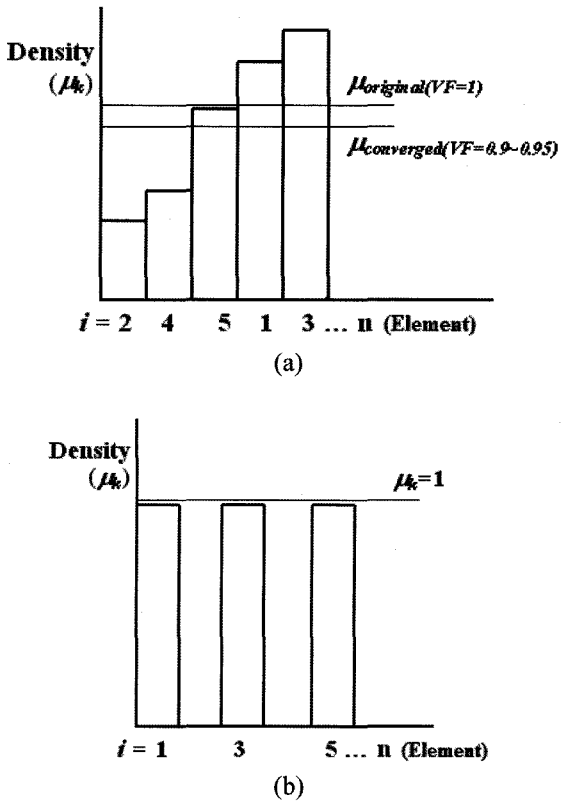

Figure 3. Modified scheme of Mayer's method: (a) After resizing and sorting algorithm; (b) New design after elements, some percentage of total objective area, were deleted.

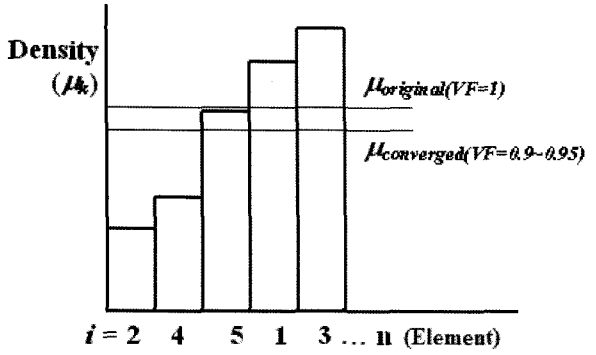

(a)

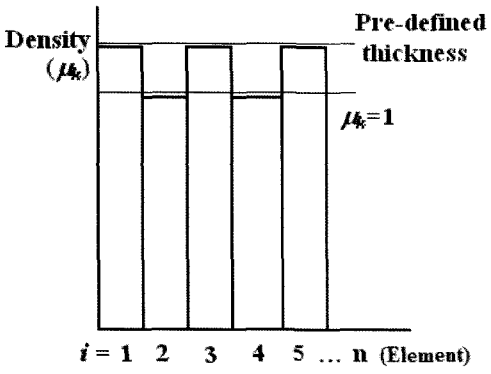

(b)

Figure 4. Modified scheme for reinforcement design: (a) After resizing and sorting algorithm; (b) In new design, the high strained elements, some.

The resizing algorithm using equations (26) and (27) satisfies specified volume constraints, VF, in equation (8), then the resizing algorithm stop. Figure 2 shows the density, $\mu^{(e)}$, of each element.

The next step is deciding the low-density elements that become the crush initiator. Mayer (1994) used the threshold algorithm that the low-density elements are deleted below the threshold value, T. But Mayer's guide-line of VF = 0.55~0.7, and T = 0.30, occasionally showed divergence. Through further studies (Cho, 2002) on convergence, we have found that convergence of resizing algorithm is more stable when used 0.90~0.95 of VF. And we change the threshold algorithm with the percentage, EN_{de}, of the total objective elements for deciding the low strain elements. The illustration of the revised algorithm is shown in Figure 3, where it is compared Mayer' scheme.

In this paper, the reverse way of Figure 3(b) that high strained elements become to be reinforced is used instead of the low strained elements to be deleted. The thickness of the high strained selected elements will be increased to absorb the more crash energy. The illustration of this revised scheme is shown in Figure 4.

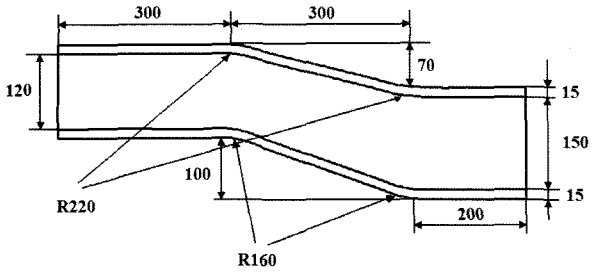

(a) Side view of example model

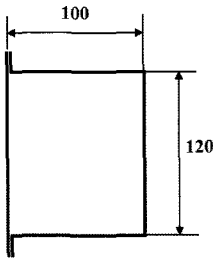

(b) Section view

Figure 5. Dimension of example model; unit mm.

3. OPTIMIZATION RESULTS

3.1. Example Model

The example model in this study was the thin-walled S-shaped member with a closed-hat section. The shape and detailed dimensions are given Figure 5. The width of flange was 15 mm. The aspect ratio, a/b, of cross-section without flange was 0.833 at front, 0.667 at rear and 0.667~0.833 at middle. The member with lumped mass, 400 kg, attached at the rear end was impacted perpendicular on rigid wall. The rigid wall was a sliding tangential to wall with finite friction, 0.15, and the rear end of model was not clamped. The model was made of sheet metal steel with mechanical of Young's modulus E = 207.0 kN/mm^2, Poisson's ratio ν = 0.3, yield stress σ_y = 0.184 kN/mm^2, plastic modulus E_p = 0.424 kN/mm^2. This model was analyzed during 30 ms using an explicit nonlinear finite element code PAM-CRASH.

According to FMVSS 208 regulation and NCAP (New Car Assessment Program) of NHTSA, the example model was impacted to perpendicular rigid wall by 25 mph, 30 mph and 35 mph with five thickness cases.

3.2. The Effect of Mass and Size of Reinforcement Design

In this chapter, the relationship of the reinforcement design for various impact velocities, V, was studied due to the fact that one crash design usually used for all impact velocities. We conducted analysis on only two thickness, 2.0 mm and 2.5 mm. And the relationship results

Table 1. Factor and level of $L_{16}(4^5)$ orthogonal array; V = 25, 30 and 35 mph, t = 2.0, 2.5 mm.

Factor	Level			
	1	2	3	4
A. EN_{up}	3.5%	7.0%	10.5%	14.0%
B. M_{up}	3.5%	7.0%	10.5%	14.0%
e*.	–	–	–	–
e*.	–	–	–	–
e*.	–	–	–	–

*Empty factors are identified by e

Table 2. Analysis Results of $L_{16}(4^5)$; P_{md} (Ton/kg).

Exp. No.	t = 2.0 mm			t = 2.5 mm		
	25 mph	30 mph	35 mph	25 mph	30 mph	35 mph
Base	0.457	0.380	0.459	0.508	0.412	0.414
1	0.466	0.458	0.485	0.419	0.541	0.573
2	0.475	0.464	0.474	0.458	0.526	0.539
3	0.472	0.479	0.567	0.513	0.504	0.556
4	0.477	0.481	0.520	0.531	0.502	0.542
5	0.488	0.475	0.468	0.407	0.507	0.554
6	0.518	0.493	0.506	0.505	0.521	0.584
7	0.479	0.509	0.545	0.516	0.536	0.584
8	0.452	0.515	0.564	0.517	0.530	0.556
9	0.485	0.464	0.474	0.447	0.520	0.529
10	0.514	0.511	0.490	0.497	0.555	0.535
11	0.548	0.576	0.486	0.514	0.590	0.555
12	0.486	0.509	0.492	0.497	0.552	0.546
13	0.410	0.456	0.495	0.438	0.433	0.469
14	0.482	0.532	0.487	0.435	0.507	0.491
15	0.502	0.569	0.561	0.484	0.559	0.575
16	0.606	0.552	0.547	0.490	0.623	0.664

pertaining to the best reinforcement design of three impact velocities that aimed at increasing the absorption of crash energy was applied to the other thickness cases.

One-step optimization was used. In the DOE method, the fractional factorial design using $L_{16}(4^5)$ orthogonal array was used. The factor and level of orthogonal array are listed in Table 1. The mass, same as thickness, of the reinforcement is defined by the percentage of total mass, M_{up}, of member. In this analysis, the thickness of reinforced elements was increased to be equivalent with M_{up}. The size of the reinforcement, EN_{up}, is defined by the percentage of total area of member negleting welding flange.

Analysis results were compared with the dynamic mean crushing load, which is the given rigid wall force by crash program. As each case of $L_{16}(4^5)$ orthogonal

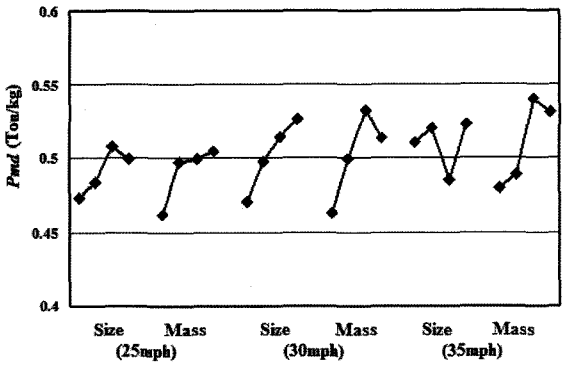

(a) t=2.0mm

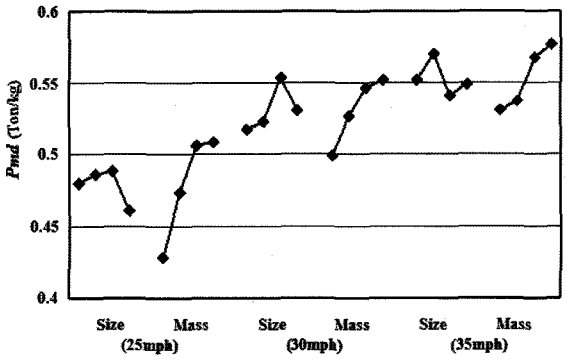

(b) t=2.5mm

Figure 6. Factor effects for t = 2.0 mm and 2.5 mm; V = 25 mph, 30 mph and 35 mph.

Table 3. Modified levels of $L_{16}(4^5)$ orthogonal array; V = 25, 30 and 35 mph for t = 2.0, 2.5 mm.

Factor	Thick-ness (mm)	Impact velocity (mph)	Level			
			1	2	3	4
A. EN_{up}	2.0	25	10.5%	14.0%	17.5%	21.0%
		30	14.0%	17.5%	21.0%	24.5%
		35	10.5%	14.0%	17.5%	21.0%
	2.5	25	3.5%	7.0%	10.5%	14.0%
		30	17.5%	21.0%	24.5%	28.0%
		35	10.5%	14.0%	17.5%	21.0%
B. M_{up}	2.0	25	10.5%	14.0%	17.5%	21.0%
		30	10.5%	14.0%	17.5%	21.0%
		35	10.5%	14.0%	17.5%	21.0%
	2.5	25	7.0%	10.5%	14.0%	17.5%
		30	10.5%	14.0%	17.5%	21.0%
		35	10.5%	14.0%	17.5%	21.0%
e.			–	–	–	–
e.			–	–	–	–
e.			–	–	–	–

Table 4. Analysis results using modified levels in Table 3; P_{md} (Ton/kg).

Exp. No.	2.0 mm			2.5 mm		
	25 mph	30 mph	35 mph	25 mph	30 mph	35 mph
Base	0.457	0.380	0.459	0.508	0.412	0.414
1	0.548	0.568	0.545	0.458	0.590	0.555
2	0.486	0.552	0.564	0.540	0.626	0.546
3	0.495	0.542	0.555	0.531	0.684	0.541
4	0.498	0.540	0.499	0.513	0.636	0.487
5	0.502	0.584	0.486	0.505	0.577	0.575
6	0.606	0.547	0.492	0.516	0.697	0.664
7	0.609	0.586	0.497	0.517	0.674	0.638
8	0.458	0.581	0.561	0.510	0.653	0.628
9	0.602	0.592	0.561	0.497	0.581	0.637
10	0.657	0.594	0.547	0.514	0.644	0.644
11	0.630	0.586	0.602	0.497	0.699	0.689
12	0.657	0.604	0.540	0.531	0.688	0.633
13	0.598	0.569	0.566	0.435	0.511	0.597
14	0.595	0.573	0.573	0.484	0.629	0.612
15	0.659	0.604	0.552	0.490	0.666	0.652
16	0.639	0.545	0.497	0.495	0.685	0.652

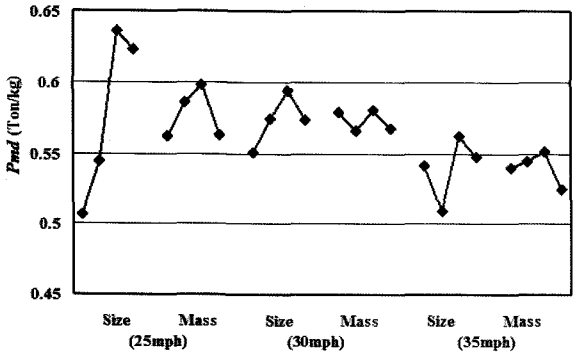

(a) t=2.0mm

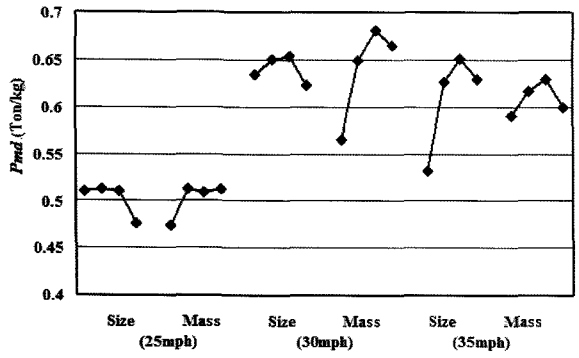

(b) t=2.5mm

Figure 7. Factor effects using modified levels for t = 2.0 mm and 2.5 mm: V = 25 mph; 30 mph; 35 mph.

array has a different mass, the average of rigid wall force per mass, P_{md}, was used.

The results of one-step optimization are listed in Table 2 and the factor effects of size, EN_{up}, and mass, M_{up}, are plotted in Figure 6. The factor effects of mass in Figure 6 showed the increasing tendency as mass of reinforcement was increased. To obtain optimum value of EN_{up} and M_{up} from the analysis results of experiment matrices in Table 2, both factors must have the convex curvature effects. Therefore, the level of EN_{up} and M_{up} in Table 1 should be changed. After several trials, the levels of both factors in Table 1 changed to those in Table 3.

Analysis results using modified levels in Table 3 are listed in Table 4. The factor effects of EN_{up} and M_{up} are plotted in Figure 7. The factor effects of M_{up} in Figure 6 are shown to have changed to convex curvature shape effects. The effect of EN_{up} is the largest except only V = 30 mph, t = 2.5 mm case.

Figure 8 shows the distribution of reinforcement that is selected by homogenization and DOE method for 2.5 mm thickness cases. For all cases of Figure 8, the selected elements, which is the dark area on the frame, to

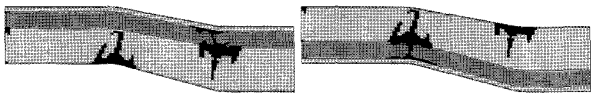

(a) Top view of 25mph (b) Bottom view of 25mph

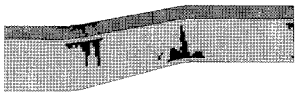

(c) Reverse view of 25mph; EN_{up}-7.0%, M_{up}-10.5%

(d) Top view of 30mph (e) Bottom view of 30mph

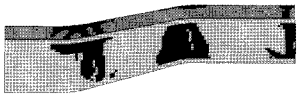

(f) Reverse view of 30mph; EN_{up}-24.5%, M_{up}-17.5%

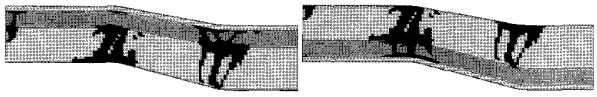

(g) Top view of 35mph (h) Bottom view of 35mph

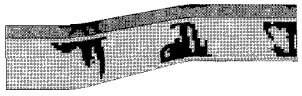

(i) Reverse view of 35mph; EN_{up}-17.5%, M_{up}-17.5%

Figure 8. Reinforcement design for t = 2.5 mm.

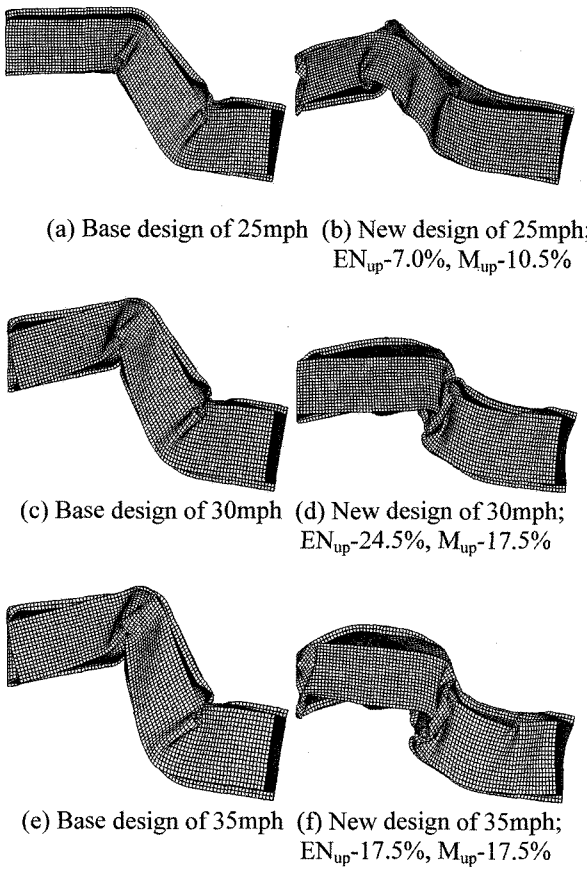

(a) Base design of 25mph (b) New design of 25mph; EN_{up}-7.0%, M_{up}-10.5%

(c) Base design of 30mph (d) New design of 30mph; EN_{up}-24.5%, M_{up}-17.5%

(e) Base design of 35mph (f) New design of 35mph; EN_{up}-17.5%, M_{up}-17.5%

Figure 9. Deformed shape comparisons at 20 ms for 2.5 mm case.

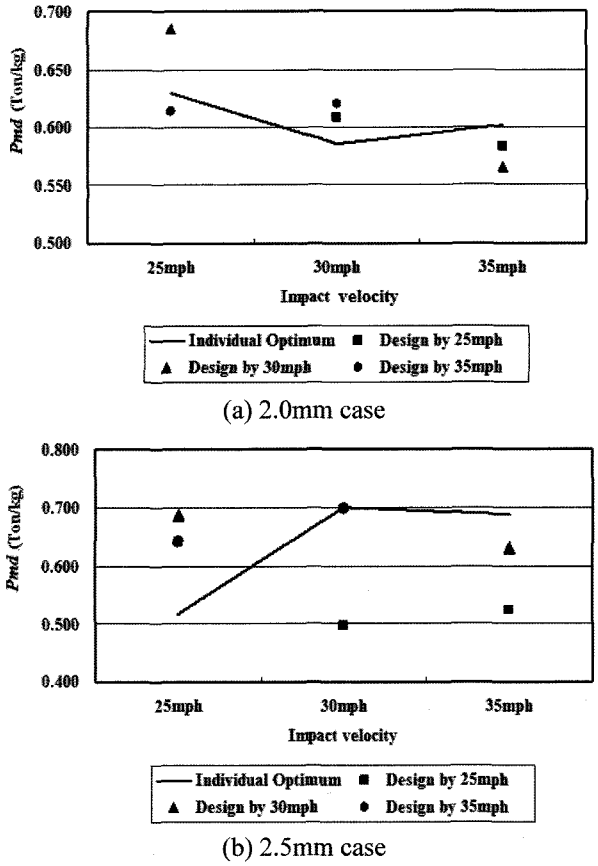

(a) 2.0mm case

(b) 2.5mm case

Figure 10. Effects of impact velocity for the new reinforcement design of 25 mph, 30 mph and 35 mph.

be reinforced similarly are located on the left side, left bottom corner and right side at the first inflection point of frame. At second inflection point, the elements to be reinforcement are located on the left top corner and right upper side of member.

Figure 9 shows the deformed shapes of base model and new reinforcement design at 20 ms for 2.5 mm cases. For the base model, bending collapse can be easily observed at the first and second inflection point of member. In the new reinforcement design case, the deformed shape was changed to the bending collapse with axial deformation that occurred between first and second inflection point in member. And the deformation became larger than the one of the base design.

3.3. The Effect of Impact Velocity for Reinforcement Design

The reinforcement designs were different according to impact velocities in previous chapter, and only one design could be applied to the front frame design. Therefore, we conducted studies on the relationship of different designs for impact velocities.

In the relationship study, a new reinforcement design, which is the optimized as shown in Figure 7, of 25 mph was run with an impact velocity of 30 mph and 35 mph. And then the deformed shape and P_{md} for each model was compared and analyzed. In the same manner, the other new reinforcement designs for 30 mph and 35 mph were analyzed.

The relationship analysis results of the reinforcement design are plotted in Figure 10. Line means the optimum results of each impact velocity. And symbols mean the results, which are analyzed different impact velocities, of reinforcement design abtained by each impact velocity. The P_{md} of the reinforcement design for 35 mph shows smaller difference than the new reinforcement design for 25 mph and 30 mph as impact velocities vary.

3.4. The Mass and Size of Reinforcement Design according to Various Thickness

In this chapter, the trend for size and thickness of reinforcement on frame according to various thicknesses were studied using the DOE method. The sample model was impacted at 35 mph using the given results from the

Table 5. Modified levels of $L_{16}(4^5)$ orthogonal array for various thickness;V = 35 mph.

Factor	Thickness (mm)	Level			
		1	2	3	4
A. EN_{up}	1.0	10.5%	14.0%	17.5%	21.0%
	1.5	10.5%	14.0%	17.5%	21.0%
	2.0	10.5%	14.0%	17.5%	21.0%
	2.5	10.5%	14.0%	17.5%	21.0%
	3.0	17.5%	21.0%	24.5%	28.0%
B. M_{up}	1.0	7.0%	10.5%	14.0%	17.5%
	1.5	7.0%	10.5%	14.0%	17.5%
	2.0	10.5%	14.0%	17.5%	21.0%
	2.5	10.5%	14.0%	17.5%	21.0%
	3.0	21.0%	24.5%	28.0%	31.5%
e.		–	–	–	–
e.		–	–	–	–
e.		–	–	–	–

previous chapter 3.1 and 3.2. One-step optimization and $L_{16}(4^5)$ orthogonal array were used. For t = 2.0 and 2.5 mm case, optimization analysis results of Chapter 3.1 were used again. For t = 1.0, 1.5 and 3.0 mm cases, the levels of factors were used same as in Table 1. After several trials, the levels of both factors were obtained and are listed in Table 5.

Table 6. Analysis results using modified levels in Table 5 ; P_{md} (Ton/kg), V = 35 mph.

Exp. No.	Thickness (mm)				
	1.0	1.5	2.0	2.5	3.0
Base	0.362	0.395	0.459	0.414	0.510
1	0.430	0.521	0.545	0.555	0.801
2	0.398	0.512	0.564	0.546	0.776
3	0.375	0.519	0.555	0.541	0.824
4	0.371	0.465	0.499	0.487	0.636
5	0.405	0.499	0.486	0.575	0.739
6	0.414	0.514	0.492	0.664	0.844
7	0.420	0.524	0.497	0.638	0.898
8	0.399	0.519	0.561	0.628	0.637
9	0.386	0.432	0.561	0.637	0.717
10	0.419	0.509	0.547	0.644	0.840
11	0.393	0.489	0.602	0.689	0.831
12	0.389	0.514	0.540	0.633	0.700
13	0.397	0.486	0.566	0.597	0.756
14	0.411	0.492	0.573	0.612	0.808
15	0.388	0.491	0.552	0.652	0.824
16	0.397	0.483	0.497	0.652	0.722

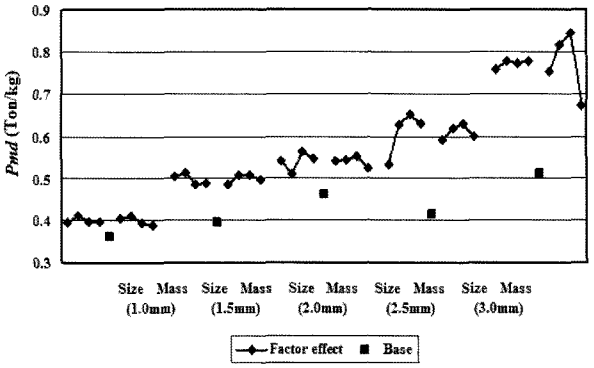

Figure 11. Factor effects for various thicknesses; V = 35 mph.

The factor effects of EN_{up} and M_{up} for five thicknesses are plotted graphically in Figure 11. The factor effect of M_{up} is seen to be the largest for t = 1.0 and 3.0 mm and the factor effect of EN_{up} is the largest for t = 1.5, 2.0 and 2.5 mm. The effect of the reinforcement is increased as the thicknesses also become thicker and specific P_{md} of optimized design in Figure 11 shows a 14%~76% increment compared with the base cases.

For t = 1.0 and 1.5 mm, the optimum conditions of EN_{up} and M_{up} are 14.0% and 10.5%. And the thickness of the reinforcement is 1.75 mm and 2.63 mm, respectively, including base thickness. For t = 2.0 and 2.5 mm, the optimum conditions of EN_{up} and M_{up} are 17.5% and 17.5%. And the thickness of the reinforcement is 4.0 mm and 5.0 mm, respectively, including base thickness. For t = 3.0 mm, the optimum conditions of EN_{up} and M_{up} are 21.0% and 28.0%, respectively, and the thickness of the reinforcement is 7.0 mm including base thickness. The size and thickness of the reinforcement shows an increasing tendency as base thickness is increased.

The reinforcement thickness of the optimum conditions is relatively large. Therefore, it is possible for the alternative method to use high strength steel for the reinforcement instead of increasing the thickness of the reinforcement. Therefore, it is necessary to study the effect of high strength steel instead of increasing the thickness of reinforcement.

Figure 12 shows the reinforcement design, which is the dark area on the frame, of various thickness cases for V=35mph. For all cases, the selected elements to be reinforcement located on the left side, left bottom corner and right side at the first inflection point of frame. At second inflection point, the reinforcement elements are located on the left top corner and right upper side of member.

Figure 13 shows the deformed shapes of the base

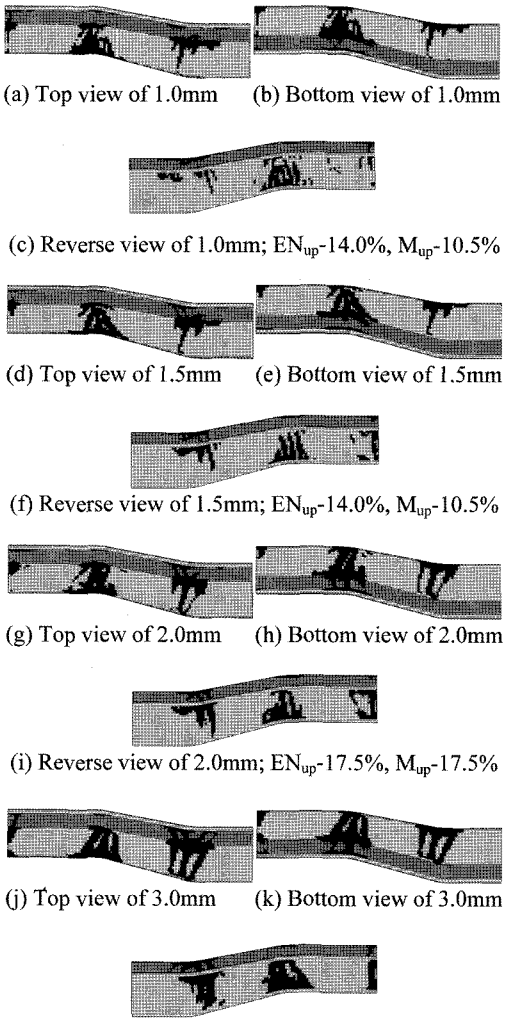

(a) Top view of 1.0mm (b) Bottom view of 1.0mm

(c) Reverse view of 1.0mm; EN_{up}-14.0%, M_{up}-10.5%

(d) Top view of 1.5mm (e) Bottom view of 1.5mm

(f) Reverse view of 1.5mm; EN_{up}-14.0%, M_{up}-10.5%

(g) Top view of 2.0mm (h) Bottom view of 2.0mm

(i) Reverse view of 2.0mm; EN_{up}-17.5%, M_{up}-17.5%

(j) Top view of 3.0mm (k) Bottom view of 3.0mm

(l) Reverse view of 3.0mm; EN_{up}-21.0%, M_{up}-28.0%

Figure 12. Reinforcement design for V = 35 mph.

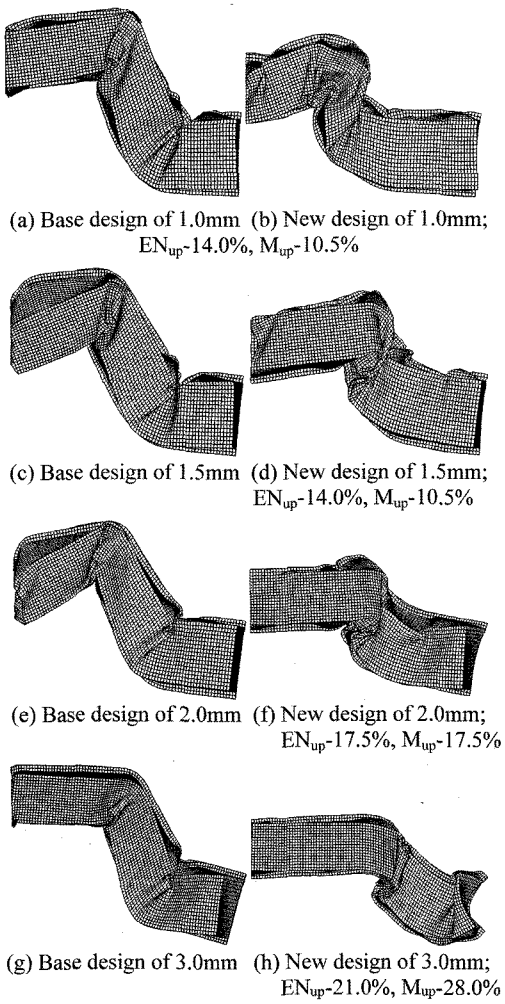

(a) Base design of 1.0mm (b) New design of 1.0mm; EN_{up}-14.0%, M_{up}-10.5%

(c) Base design of 1.5mm (d) New design of 1.5mm; EN_{up}-14.0%, M_{up}-10.5%

(e) Base design of 2.0mm (f) New design of 2.0mm; EN_{up}-17.5%, M_{up}-17.5%

(g) Base design of 3.0mm (h) New design of 3.0mm; EN_{up}-21.0%, M_{up}-28.0%

Figure 13. Deformed shape comparison at 20 ms; V = 35 mph.

model and new reinforcement design at 20 ms for 35mph cases. The new reinforcement design is seen to have changed the bending collapse position of the base model, which occurred at the first and second inflection point of the frame to mid area of the first and second inflection point in member, and also, is deformed more than the base design.

3.5 Comparison of the Optimum Mass and Size of Reinforcement Design using DOE and RSM

If a factional factorial design using the orthogonal array is used to obtain optimized design, it can be obtained a sensitivity and approximate optimum of design factors with relatively few analyses, but the only disadvantage of this method is that it is unable to obtain an accurate optimum. Therefore, in this study, to compare an optimum value obtained using factional factorial design

Table 7. Modified levels of $L_9(3^4)$ orthogonal array for various thickness; V = 35 mph.

Factor	Thickness (mm)	Level		
		1	2	3
A. EN_{up}	1.0	10.5%	14.0%	17.5%
	1.5	10.5%	14.0%	17.5%
	2.0	14.0%	17.5%	21.0%
	2.5	14.0%	17.5%	21.0%
	3.0	17.5%	21.0%	24.5%
B. M_{up}	1.0	7.0%	10.5%	14.0%
	1.5	7.0%	10.5%	14.0%
	2.0	14.0%	17.5%	21.0%
	2.5	14.0%	17.5%	21.0%
	3.0	24.5%	28.0%	31.5%
e.		–	–	–
e.		–	–	–

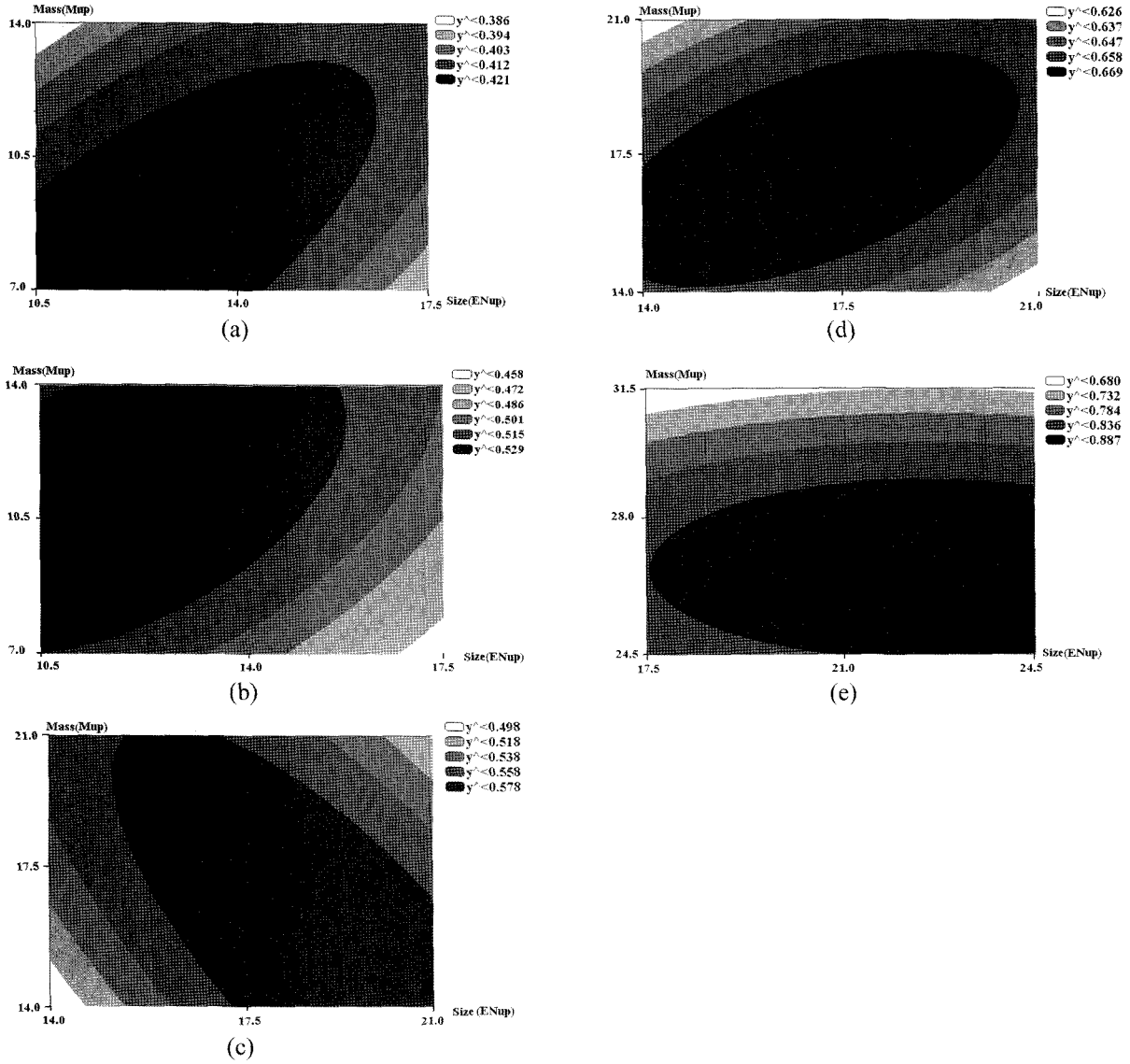

Figure 14. Response surface contour plot for each thickness; V = 35 mph: (a) Response surface contour plot for t=1.0 mm; (b) Response surface contour plot for t=1.5 mm; (c) Response surface contour plot for t=2.0 mm; (d) Response surface contour plot for t=2.5 mm; (e) Response surface contour plot for t=3.0 mm.

Table 8. Comparison of optimum size and mass of reinforcement by DOE and RSM.

Thick-ness (mm)	Base	By DOE (Table 6)			By RSM			
					Predicted results			Analy-sis
	P_{md}	EN_{up}	M_{up}	P_{md}	EN_{up}	M_{up}	P_{md}	P_{md}
1.0	0.362	14.0	10.5	0.414	12.3	7.99	0.421	0.435
1.5	0.395	14.0	10.5	0.514	11.9	11.0	0.529	0.524
2.0	0.459	17.5	17.5	0.602	19.5	14.9	0.578	0.550
2.5	0.414	17.5	17.5	0.689	17.0	17.2	0.669	0.684
3.0	0.510	21.0	28.0	0.898	22.6	26.7	0.887	0.876

with the orthogonal array and the RSM ethod with second order regression model was used. Also, the trend curve for the optimum size and thickness of the reinforcement according to various base thicknesses of model were studied.

Because the second order regression model in RSM using orthogonal array requires a 3-level for each factor, new $L_9(3^4)$ orthogonal array were used. Levels of $L_9(3^4)$ orthogonal array were modified and are tabulated in Table 7.

The response contour surface of each thickness is plotted graphically in Figure 14 using data in Tables 6 and 7. The optimum EN_{dc} and M_{up} given by RSM were

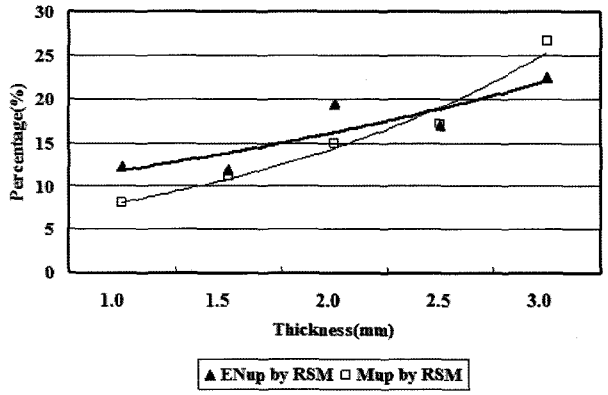

Figure 15. Trend curve of the predicted optimum EN_{de} and M_{up} given by RSM.

compared with the DOE results of Figure 14 and are listed in Table 8. The optimum EN_{de} and M_{up} given by the RSM method is shown to be similar to the results obtained from using the DOE method. The difference of specific dynamic mean crushing load between predicted results and analysis results, as listed in Table 8, using the RSM method is below 5%. The specific dynamic mean crushing load of analysis results by RSM is 1~9% different with the results obtained from using the DOE method.

The trend curve of EN_{up} and $M_{up,}$ using the results obtained from the RSM method, as shown in Table 8, is plotted graphically in Figure 15. The size and thickness of the reinforcement show increasing tendency to absorb more crash energy as thickness of base model is increased. Also, the reinforcement is more effective way than increasing the thickness of whole model is confirmed.

4. CONCLUSIONS

In this paper, the frontal crash optimization of S-shaped closed-hat section member using the homogenization method and the DOE method was studied. The optimization was studied to introduce the reinforcement. The optimum size and thickness of the reinforcement was the main focus here. In this study, the location of the reinforcement, which were the highly strained elements of the sample model, was decided by the homogenization method. Also, the effective size and thickness of reinforcements was studied by the DOE and the RSM methods.

The relationship of the reinforcement design according to various impact velocities was studied. The reinforcement design of higher impact velocities showed to absorb more crash energy than low velocities design.

The size and thickness of reinforcements for various thicknesses were studied using design of experiments and response surface method. The factor effect of reinforcement size was large for medium thickness of base model and the factor effect of reinforcement thickness was large for week and relatively thick thickness cases of base model. The optimum size and thickness had an increasing tendency as the thickness of base model was increased. Also, as the thickness of the base model was increased, the effect of optimization using reinforcement also showed an increasing tendency.

The approximate trend curve for effective size and thickness of reinforcement using response surface method was studied. The predicted size and thickness of reinforcement by RSM were compared with the results of the DOE method. The specific dynamic mean crushing loads of predicted design by RSM were compared to the predicted results by the RSM and DOE results. From these compared results, the closed relationship for those designs was shown. Therefore, these results can be used to find the optimum reinforcement design for S-shape front frame of vehicle as the base guideline.

The optimized designs of reinforcement showed checkerboard pattern; therefore, it is not easy to make reinforcement in real manufacturing process. Therefore, it is necessary to conduct studies on the simple shape reinforcement, which is an equivalent size of optimized design Also, as the thickness value of optimized reinforcement design was given relatively large, the effect of the high strength steel for reinforcement instead of the thickness design must be studied.

To adopt conveniently and confidently above results in this paper, various examples like that are various aspect ratio of cross section, the offset height of S-frame and etc should be studied. Also, the results of reinforcement design for component model should be applied and compared to full scale model.

REFERENCES

Abe, K., Ohta, M. and Takagi, M. (1990). Collapse of thin-walled curved beam with closed-hat section – Part 2: Simulation by plane plastic hinge model. *SAE Paper No. 900461*.

Bendsoe, M. P. and Kikuchi, N. (1988). Generating optimal topologies in structural design using a homogenization method. *Computer Methods in Applied Mechanics and Engineering*, **71**, 197–224.

Cho, Y. B. and Sin, H. C. (2001). A basic study of crashworthiness optimization using homogenization method(I). *Trans. Korean Society of Automotive Engineers* **9**, **3**, 190–200.

Cho, Y. B. and Sin, H. C. (2002). A basic study of crashworthiness optimization using homogenization method(II). *Trans. Korean Society of Automotive Engineers* **10**, **4**, 181–191.

Cho, Y. B. (2002). Crashworthiness optimization of a

closed-hat section member using homogenization method and design of experiments. *Ph.D Dissertation. Seoul National University*, Seoul.

Drazetic, P., Markiewicz, E. and Ravalard, Y. (1993). Application of kinematic models to comparison and bending in simplified crash calculation. *Int. J. Mech. Sci.* **35, 3/4**, 179–191.

Elmarakbi, A. M. and Zu, J. W. (2004). Dynamic modeling and analysis of vehicle smart structures for frontal collision improvement. *Int. J. Automotive Technology* **5, 4**, 247–255.

Guedes, J. M. and Kikuchi, N. (1990). Preprocessing and postprocessing for materials based on the homogenization method with adaptive finite element method. *Computer Methods in Applied Mechanics and Engineering*, **83**, 143–198.

Kim, H. S. and Wierzbicki, T. (2001). Effect of the cross-sectional shape of hat-type cross-sections on crash resistance of an "S"-frame. *Thin-walled Structures*, **39**, 535–554.

Ma, Z., Kikuchi, N., Pierre, C. and Raju, B. (2004). Multi-domain multi-step topology optimization for vehicle structure crashworthiness design. *SAE Paper No.* 2004-01-1173.

Mayer, R. R. (1994). Application of topological optimization techniques to structural crashworthiness. *Ph.D Dissertation, University of Michigan*, Ann Arbor.

Mayer, R. R. and Kikuchi, N. (1996). Application of topological optimization techniques to structural crashworthiness. *Int. J. Numerical Method in Engineering*, **39**, 1383–1403.

Min, S. and Kikuchi, N. (1997). Optimal reinforcement design of structures under the buckling load using the homogenization design method. *Structural Engineering Mechanics* **5, 5**, 565–576.

Myers, R. H. (1971). *Response Surface Methodology.* Allyn and Bacon Inc.. Boston.

Ohkami, Y., Takada, K., Motomura, K., Shimamura, M., Tomizawa, H. and Usuda, M. (1990). Collapse of thin-walled curved beam with closed-hat section – Part 1: Study on collapse characteristics. *SAE Paper No.* 900460.

Phadke, M. S. (1989). *Quality Engineering Using Robust Design*. Prentice Hall. New Jersy.

Qi, C., Ma, Z., Kikuchi, N., Pierre, C., Wang, H. and Raju, B. (2005). Fundamental studies on crashworthiness design with uncertainties in the system. *SAE Paper No.* 2005-01-0613.

Suzuki, K and Kikuchi, N. (1991). A homogenization method for shape and topology optimization. *Computer Methods in Applied Mechanics and Engineering*, **93**, 291–318.

Taguchi, G. (1987). *System of Experimental Design* **1** and **2**. UNIPUB/Kraus International Publications. New York.

Taguchi, G. (1987). *Introduction to Quality Engineering.* American Supplier Institute Inc.. Michigan.

Wang, H. C. and Meredith, D. (1994). The crush analysis of vehicle structures. *Int. J. Impact Engng.* **1, 3**, 199–225.